Electrochemical and Surface Study of Ferrocenoyl Oligopeptides

Irene Bediako-Amoa, Todd C. Sutherland, Chen-Zhong Li, Roberta Silerova, and Heinz-Bernhard Kraatz*

Department of Chemistry, University of Saskatchewan, 110 Science Place, Saskatoon, Saskatchewan, Canada S7N 5C9

Received: September 26, 2003; In Final Form: October 27, 2003

The syntheses and characterizations of several symmetric ferrocenoyl (Fc)−peptide cystamines ([Fc-Gly-CSA]$_2$, [Fc-Ala-CSA]$_2$, [Fc-Ala-Ala,CSA]$_2$, [Fc-Ala-Phe-CSA]$_2$, together with an unsymmetric Fc-Ala-Ala-CSA-Ala-Fc) is reported. All systems show intermolecular hydrogen bonding in solution. In the solid-state, [Fc-Gly-CSA]$_2$ and [Fc-Ala-CSA]$_2$ exhibit strong intermolecular H-bonding, as expected from solution studies, forming a network of β-helical supramolecular structures. Monolayers of the Fc−peptide cystamines produced structures that show a uniform thickness of 7(2) Å but are not well ordered, leaving about 10−15% of the Au surface exposed as determined by Cu underpotential deposition. $E^{0\prime}$ values of all the monolayers are in the range of 460−510 mV. Monolayer dilution with hexanethiol caused an anodic redox shift of approximately 20 mV and a slight increase in the electron-transfer kinetics.

Introduction

An understanding of the fundamental properties that govern redox processes in biological systems remains elusive at the molecular level. To this end, electron transfer (ET) from a donor to an acceptor through structurally well-defined peptide spacers has been studied by various groups using photophysical techniques in solution. However, the lack of structural information and the flexibility of the peptide spacer often complicate data analysis.[1−8] A large step forward was provided by electrochemical measurements of the ET process on redox-labeled thiol monolayers.[9−18] Formation of monolayers, via the Au−thiolate bond, forces the ET to occur through the spacer. In addition, ET reactions are monitored in both the forward and reverse directions, which allows for monitoring of possible rectification.

Given these benefits and the few of studies of ET in peptides by electrochemical methods, we decided to embark on a detailed study of the role of a peptide spacer on ET processes, with the aim of relating the information back to biological systems. We recently reported a detailed study on a series of *N*-ferrocenoyl (Fc)-labeled oligoproline cystamines [Fc-Pro$_n$-CSA]$_2$ (Pro = proline, CSA = cystamine, n = 0−6) possessing polyproline II structure.[19] These peptide conjugates form well-behaved and stable monolayers on gold aided by potential hydrogen bonding to adjacent molecules. The ET between the Fc redox probe and a gold microelectrode surface across the oligoproline spacer was examined, showing a distance-dependent k_{ET}, which deviates significantly from Marcus-type behavior, implicating a through-bond mechanism for the ET process.

Fc−peptide systems are known to exhibit interesting structures in the solid state. The incorporation of a disulfide not only enables the attachment to surfaces but also has yielded novel structural peptide motifs.[20−25] Hirao has developed systems using 1,1′-Fc−peptides that show strong intramolecular H-bonding in the solid state,[26−32] leading to chiral helical supramolecular arrangements that do not rely on intermolecular H-bonding but are the result of chiral patterning. Recent results from our laboratory[33] of a simple Fc peptide, (Fc-Gly-CSA)$_2$ (Gly = glycine), have revealed a strong intermolecular H-bonded network in the solid state displaying a chiral double helical system, including a twisted β-helix with the helices decorated with redox-active Fc groups. This molecule is not only structurally interesting but also serves as the starting point for our present study, in which we decided to investigate the solution and surface electrochemical properties of simple Fc−peptide cystamines, which are unable to adopt a stable secondary structure. For this purpose, we have studied simple amino acids such as alanine (Ala), dialanine (Ala$_2$), and phenylalanine−alanine (Phe-Ala) as spacers, which provide a limited variation in the length of the peptide spacer. This paper gives a full account of our work with the short Fc−peptide cystamines, [Fc-Gly-CSA]$_2$ (**5**), [Fc-Ala-CSA]$_2$ (**6**), [Fc-Ala$_2$−CSA]$_2$ (**7**), [Fc-Phe-Ala-CSA]$_2$ (**8**), and Fc-Ala-CSA$_2$−Ala$_2$−Fc (**9**). We report their synthesis and full characterization, including the crystal structure of compound **6** and provide full details of our surface electrochemical studies.

Experimental Section

(a) Characterization (for Synthetic Details, See Supporting Information). [Fc-Gly-CSA]$_2$ (5). Anal. Calcd for $C_{30}H_{34}O_4N_4S_2Fe_2 \cdot CH_2Cl_2$: C, 46.45; H, 4.39; N, 7.32. Found: C, 46.55; H, 4.77; N, 7.99. LRMS−FAB: $[M + 1]^+$ calcd, 690; found, 691; 129 (10), 185 (25), 213 (100), 364 (24), 625 (15), 691 (80). FTIR ($CHCl_3$, [**5**] = 6 mM cm^{-1}): 1658 (C═O Gly), 1640 (C═O Fc). ^{1}H NMR ($CDCl_3$): 7.58 (1 H, t, J_{HH} = 6.0 Hz, NH CSA), 7.31 (1 H, t, J_{HH} = 5.0, NH Gly), 4.83 (2H, s, CH_o Cp), 4.35 (2 H, s, CH_m Cp), 4.21 (5 H, s, Cp), 4.05, (2 H, d, J_{HH} = 5.5, CH_2 Gly), 3.60 (2 H, m, $^{\beta}CH_2$ CSA), 2.75 (2 H, t, J_{HH} = 6.5, $^{\alpha}CH_2$ CSA). ^{13}C NMR ($CDCl_3$): 172.1 (C═O CSA), 170.5 (C═O Gly), 75.4 (C_i Cp), 70.9 (CH_m Cp), 70.0 (C of Cp), 68.7 (CH_o Cp), 43.8 (CH_2 Gly), 38.9 ($^{\beta}CH_2$ CSA), 38.4 ($^{\alpha}CH_2$ CSA). λ_{max} nm (ϵ/dm^3 mol^{-1} cm^{-1}) = 442 (200).

[Fc-Ala-CSA]$_2$ (6). Anal. Calcd for $C_{32}H_{38}O_4N_4S_2Fe_2 \cdot {}^1/_2CH_2Cl_2$: C, 49.34; H, 4.84; N, 7.18. Found: C, 49.34; H, 4.23; N, 7.06. LRMS−FAB: $[M + 1]^+$ calcd, 718; found, 719; 185 (15),

* Author to whom correspondence may be addressed. E-mail: kraatz@sask.usask.ca.

10.1021/jp0368785 CCC: $27.50
Published on Web 12/05/2003

213 (86), 360 (20), 653 (17), 719 (100). FTIR ($CHCl_3$, [**6**] = 6 mM cm^{-1}): 1663 (C═O Ala), 1636 (C═O Fc). ^1H NMR ($CDCl_3$): 7.73 (1 H, t, J_{HH} = 8.0 Hz, NH CSA), 7.04 (1 H, d, J_{HH} = 8.0 Hz, NH Ala), 4.89 (1 H, s, CH Ala), 4.80 (2 H, s, CH_o Cp), 4.34 (2 H, s, CH_m Cp), 4.20 (5 H, s, Cp), 3.70−3.35 (2 H, m, $^{\beta}CH_2$ CSA), 2.80 (2 H, m, $^{\alpha}CH_2$ CSA), 1.75 (1 H, broad, CH_3 Ala), 1.50 (3 H, d, J_{HH} = 6.9 Hz, CH_3, Ala). ^{13}C NMR ($CDCl_3$): 173.7 (C═O CSA), 171.1 (C═O Ala), 75.4 (C_i Cp), 70.9 (C of Cp), 70.0 (CH_m substitut. Cp), 68.9 (CH_o, C substitut. Cp), 68.6 (CH_o, substitut. Cp), 48.7 (CH, Ala), 38.9 ($^{\beta}$CH2, CSA), 38.5 ($^{\alpha}$CH2, CSA), 18.6 (CH_3, Ala), 14.4 (CH_3, Ala). λ_{max} nm (ϵ/dm^3 mol^{-1} cm^{-1}) = 444 (380).

[Fc-Ala$_2$-CSA]$_2$ (7). Anal. Calcd of $C_{32}H_{38}O_4N_4S_2Fe_2 \cdot {}^1/_2CH_2Cl_2$: C, 46.53; H, 4.89; N, 8.57. Found: C, 46.50; H, 4.55; N, 8.23. LRMS−FAB: $[M + 1]^+$ calcd, 860; found, 861; 107 (40), 154 (100), 213 (85), 284 (15), 860 (15). FTIR ($CHCl_3$, [**7**] = 6 mM cm^{-1}): 1652 (br, C═O Ala), 1646 (C═O Fc). ^1H NMR ($CDCl_3$): 7.65 (1 H, t, J_{HH} = 7.5 Hz, NH CSA), 7.45 (1 H, d, J_{HH} = 7.5 Hz, NH Ala), 6.88 (1 H, d, J_{HH} = 7.7 Hz, NH Ala), 4.85 (1 H, J_{HH} = 6.0, CH Ala), 4.75−4.70 (2 H, br s, CH_o to Cp), 4.32 (1 H, m, CH Ala), 4.22 (2 H, s, CH_m Cp), 4.20 (5 H, s, Cp), 3.70−3.40 (2 H, m, $^{\beta}CH_2$ CSA), 2.80 (2 H, m, $^{\alpha}CH_2$ CSA) 1.48 (3 H, d, J_{HH} = 6.8 Hz, CH_3 Ala), 1.40 (3 H, d, J_{HH} = 6.8 Hz, CH_3 Ala). ^{13}C NMR ($CDCl_3$): 173.2 (C═O), 171.0 (C═O), 162.2 (C═O), 75.3 (C_i Cp), 71.1 (CH_m Cp), 70.1 (C of Cp), 68.7 (CH_o Cp), 68.5 (CH_o Cp), 49.1 (CH, Ala), 48.8 (CH, Ala), 38.8 ($^{\beta}CH_2$, CSA), 37.6 ($^{\alpha}CH_2$, CSA), 25.9 (CH_3 of Ala), 18.8 (CH_3, Ala). λ_{max} nm (ϵ/dm^3 mol^{-1} cm^{-1}) = 443 (550).

[Fc-Phe-Ala-CSA]$_2$ (8). Anal. Calcd for $C_{50}H_{56}O_6N_6S_2Fe_2 \cdot CH_2Cl_2$: C, 55.13; H, 5.23; N, 7.38. Found: C, 55.97; H, 5.22; N, 7.83. LRMS−FAB: $[M + 1]^+$ calcd, 1012; found, 1013. FTIR ($CHCl_3$, [**8**] = 6 mM cm^{-1}): 1682 (br, C═O Phe-Ala), 1639 (C═O Fc). ^1H NMR ($CDCl_3$): 7.90 (1 H, br s, NH CSA), 7.51−7.05 (5 H, m, H Phe), 6.58 (1 H, d, J_{HH} = 7.0 Hz, NH Phe), 5.35 (1 H, br s, NH Ala), 4.96−4.90 (2 H, s, CH_o Cp), 4.50 (1 H, m, CH Phe), 4.30 (1 H, br s, CH Ala), 4.28 (2 H, s, CH_m Cp), 4.01 (5 H, s, Cp), 3.65−3.35 (2 H, m, CH_2 Phe), 3.32−3.14, (2 H, m, $^{\beta}CH_2$ CSA), 2.75 (2 H, m, $^{\alpha}CH_2$ CSA), 1.34 (3 H, d, J_{HH} = 7.0 Hz, CH_3 Ala). ^{13}C NMR ($CDCl_3$): 175.1 (C═O CSA), 172.6 (C═O Phe), 171.4 (C═O Ala), 137.0 (C_i Phe), 129.5 (CH, Phe), 129.1 (CH, Phe), 127.2 (CH, Phe), 74.7 (C_i Cp), 71.1 (CH_m Cp), 70.0 (C of Cp), 69.2 (CH_o Cp), 67.8 ((CH_o Cp), 55.2 (CH, Phe), 49.3 (CH, Ala), 38.9 (CH_2, Phe), 38.5 ($^{\beta}CH_2$ CSA), 38.0 ($^{\alpha}CH_2$, CSA), 18.6 (CH_3, Ala). λ_{max} nm (ϵ/dm^3 mol^{-1} cm^{-1}) = 443 (310).

Fc-Ala-CSA$_2$-Ala$_2$-Fc (9). Anal. Calcd for $C_{35}H_{43}O_5N_5S_2Fe_2 \cdot CH_2Cl_2$: C, 49.54; H, 4.84; N, 8.04. Found: C, 48.83; H, 4.89; N, 8.11. LRMS−FAB: $[M + 1]^+$ calcd, 788; found, 789; 71 (43), 136 (70), 213 (100), 284 (20), 360 (10), 507 (10), 724 (15), 792 (65). FTIR ($CHCl_3$, [**9**] = 6 mM cm^{-1}): 1663 (br, C−O Ala), 1640 (C−O Fc). ^1H NMR ($CDCl_3$): 7.52 (1 H, br S, NH CSA), 6.78 (1 H, d, J_{HH} = 8.0 Hz, NH Ala), 6.58 (1 H, d, J_{HH} = 7.8 Hz, NH Ala), 4.79 (1 H, br s, CH Ala), 4.76 (1 H, br s, CH Ala), 4.73 (2 H, s, CH_o Cp), 4.56 (2 H, br s, CH_m Cp), 4.20 (5 H, s, Cp), 3.40−3.70 (2 H, m, $^{\beta}CH_2$ CSA), 2.80 (2 H, m, $^{\alpha}CH_2$ CSA), 1.44 (∼1 H, d, J_{HH} = 6.8 Hz, CH_3 Ala), 1.23 (∼3 H, d, J_{HH} = 7.1 Hz, CH_3 Ala). ^{13}C NMR ($CDCl_3$): 173.6 (C═O), 173.0 (C═O), 171.0 (C═O), 75.2 (C_i Cp), 71.1 (CH_m Cp), 70.1 (C of Cp), 68.8 (CH_o Cp), 68.6 (CH_o Cp), 49.6 (CH Ala), 49.3 (CH Ala), 38.9 ($^{\beta}CH_2$ CSA), 37.9 ($^{\alpha}CH_2$ CSA), 19.0 (CH_3 of Ala), 18.8 (CH_3 Ala), 18.4 (CH_3 of Ala). λ_{max} nm (ϵ/dm^3 mol^{-1} cm^{-1}) = 442 (200).

(b) Electrochemistry. *Solution Electrochemistry.* All solution electrochemical measurements were carried out on a CV-50W voltammetric analyzer (BAS) at room temperature (22 ± 3 °C). Tetrabutylammonium perchlorate (TBAP, 0.1 M) was used as supporting electrolyte, glassy carbon (BAS) was the working electrode (diameter 3 mm), Pt wire was the counter electrode, and Ag/AgCl/3.0 M KCl (BAS) was used as the reference electrode. IR compensation was applied. For each of the ferrocenoyl−peptide cystamine solutions at 1 mM in CH_3CN/TBAP, five replicate measurements were recorded at the same scan rate (50−500 mV/s) over a potential range of 100−900 mV.

Surface Electrode Preparation. Microelectrodes were prepared by inserting a gold wire (diameter of 50 μm) into a glass capillary tube (outer diameter = 1.5 mm); the gold wire was 0.5 cm longer than the capillary tube on both sides. The capillary tube was heated at the midpoint six consecutive times for 20 s each time until it melted into the gold wire. The glass capillary tube was cut at its midpoint. An insulated wire approximately 1 cm longer than the glass capillary tube was also fixed inside the capillary tube. Silver conductive ink was used as a contact to bridge the gold wire and wrapping wire in the capillary tube. The capillary tube was fixed inside shrink-wrap tubing (about two-thirds the length of the capillary tube) and heated until it was tightly fixed around the capillary tube. The capillary tube was fixed such that it covered the gold wire. The microelectrodes were polished first on a diamond polishing pad to remove the glass on the gold surface then on microcloth pads with alumina slurry of three different sizes, 1, 0.3, and 0.05 μm, and rinsed with distilled water and sonicated before use.

A typical cleaning procedure for monolayer surface preparation was as follows: Gold electrodes were polished on microcloth pads as described above. Linear sweep voltammetry (LSV) of the polished electrode was run in an aqueous solution of 0.5 M KOH from 0 to −1.4 V at a scan rate of 100 mV/s. LSV was repeated until no peak for adsorbed thiol was observed. The gold electrode was then rinsed with distilled water and cycled in H_2SO_4 (0−1.4 V at 100 mV s^{-1}) until stable peaks for Au oxidation and reduction were observed and finally ended with a linear sweep to oxidize the gold electrode where it was then stored.

Under Potential Deposition. All microelectrode electrochemical experiments used a home-built potentiostat design specifically for microelectrodes.[34] Under potential deposition (UPD) of copper was used to determine the surface roughness of the gold microelectrode after cleaning and to determine the exposed gold area after monolayer formation. A potential step method using chronoamperometry was performed in 1.0 mM $Cu(ClO_4)_2 \cdot 6H_2O$ in 0.1 M $HClO_4$ from a potential of 500−0 mV for 30 s to deposit a monolayer of copper atoms on the surface of the gold electrode. After, LSV was applied to strip the copper from 150 to 500 mV at a scan rate of 100 mV/s. The amount of charge for the deposition of copper by UPD on a bare or modified gold electrode was obtained by integration of the anodic peak from LSV.

Monolayer Preparation. The stored gold electrode was immersed in deoxygenated ethanol for about 20 min to reduce the gold oxide to gold before monolayer preparation. The reduced gold electrode was immediately immersed in a 1 mM solution of the ferrocenoyl−oligopeptide cystamines **5**−**9** in ethanol. After 5 days of immersion, the electrode was sonicated in ethanol for 2 min and then rinsed with distilled water. Diluted monolayers were prepared by following the above procedure with an additional step of incubating the modified electrodes in 1 mM ethanolic solution of hexanethiol. Cyclic voltammograms (CVs) of the modified surfaces were started at the rest

potential to a vertex at 0.8 V followed by sweeps from 0.0 to 0.8 V at various scan rates. The CVs were recorded in 2.0 M $NaClO_4$ as a supporting electrolyte, Ag/AgCl/3M KCl as a reference electrode, and Pt wire as a counter electrode. Ten gold electrodes with monolayers were prepared for each compound and all experiments were carried out at room temperature (22 ± 3 °C). Blocking studies were carried out in a solution containing equimolar amounts of $K_4[Fe(CN)_6]\cdot 3H_2O$ and $K_3[Fe(CN)_6]\cdot 3H_2O$ (1 mM) and 1 M KCl as supporting electrolyte.

(c) Optical Spectroscopy. *Absorption spectra* were recorded in the range of 350−700 nm using a CARY 500 Scan-UV−vis−NIR double beam spectrophotometer and glass cuvettes of 1 cm path length. A background scan of 0.1 M TBAP in CH_3CN was recorded and subtracted from all spectra.

FTIR spectra of all ferrocenoyl−peptide cystamines **5**−**9** were recorded on a BioRad FTS-40 Fourier transform spectrometer in $CHCl_3$ at concentrations of 6.0 and 50.0 mM using a liquid cell with NaCl windows and a path length of 0.025 mm. All spectra were recorded at a temperature of 22 ± 3 °C and a resolution of 4 cm^{-1}. Scans (4096) were collected as a background spectrum of the empty liquid cell, and 8096 scans were collected for a solvent spectrum. Sample solutions of compounds **5**−**9** were injected into the cell, and 8096 scans were collected. The solvent spectrum was subtracted from the spectra of all ferrocenoyl−peptide cystamines and a baseline correction of the subtracted spectra was applied.

Ellipsometry. Film thickness was measured using an LSE Stokes ellipsometer which has a fixed angle of 70° and a fixed wavelength (632.8 nm) with a 6328-Å HeNe Laser as its light source. Gold evaporated on Si(100) was used as the substrate (Platypus Technologies) with refractive index $N_s = 0.133$, absorption index $K_f = 3.462$, and monolayer refractive index set at 1.44.

X-ray Crystallography. Suitable crystals of **6** were obtained from acetonitrile solution containing 2 M TBAP. Orange blocks suitable for X-ray crystallography were deposited after several days. Data for **6** were measured using a Siemens Smart CCD diffractometer using Mo Kα radiation (graphite monochromated) with ω scans. The structure was solved using direct methods. All non-hydrogen atoms were refined anisotropically using full-matrix least squares on F^2. The final R value for **6** was $R = 0.0839$ and $wR^2 = 0.1855$ for 9668 reflections with $I > 2\sigma(I)$ (14 136 total reflections). Crystallographic details have been summarized in Table 1.

TABLE 1: Crystal Data and Structure Refinement for 6[a]

description	orange needle
empirical formula	$C_{32}H_{38}Fe_2N_4O_4S_2$, $C_{32}H_{36}Fe_2N_4O_4S_2$, $4(C_2H_3N)$
formula weight	1599.21
temperature	193(2) K
wavelength	0.71073 Å
cryst syst	monoclinic
space group	$P2(1)$
unit cell dimensions	$a = 11.8218(10)$ Å $b = 17.0636(15)$ Å $c = 18.9362(16)$ Å $\alpha = 90°$ $\beta = 98.624(2)°$ $\gamma = 90°$
volume	3776.7(6) Å3
Z	2
density (calcd)	1.406 mg/m3
$F(000)$	1668
GOF	1.038
R, wR^2	0.0839, 0.1855

[a] Standard deviations are in parentheses.

SCHEME 1: Synthesis of Ferrocenoyl Peptides: (i) EDC, HOBt; (ii) TFA; (iii) FcOOH, EDC, HOBt; and (iv) Boc-AA

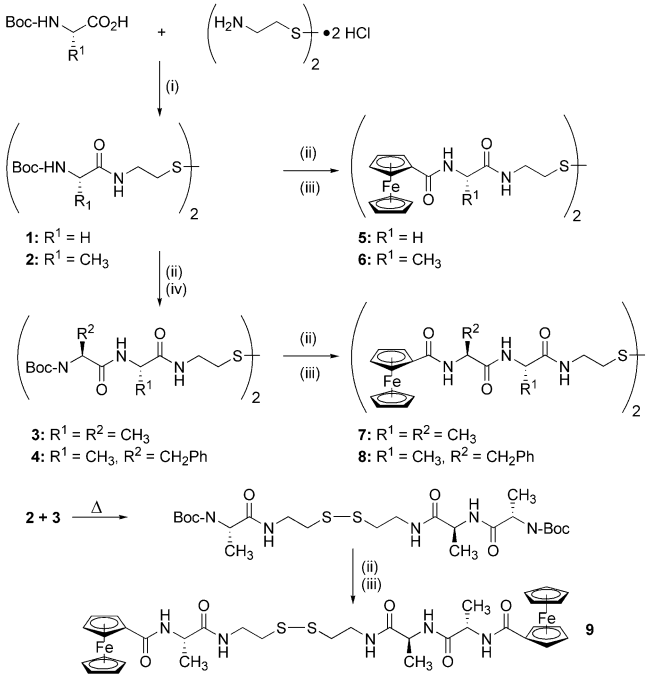

FcCOOH. Disulfides scramble readily, allowing the isolation of compound **9** in suitable yields. All Fc−peptide cystamines are yellow to orange air-stable solids, which in some cases can be crystallized from solvents to give crystals suitable for single-crystal diffraction (vide infra). Fc−peptide cystamines **5**−**8** were characterized spectroscopically by NMR, MS, and visible and elemental analyses. ^{1}H NMR assignments were based on chemical shift, integration, and signal multiplicity. In general, the chemical shifts of the Fc systems reported here compare well with those of related Fc−peptide esters.[19,37,38] In addition, a comparison of the Boc and Fc derivatives shows that upon formation of the Fc conjugate, the α H experiences a downfield shift. Interestingly, the corresponding ^{13}C signals for the α C shift slightly upfield.

The ^{1}H NMR spectra of compounds **5**−**9** exhibit the typical pattern of monosubstituted Fc systems with two signals for the

Results and Discussion

(a) Syntheses and Properties. Fc−peptide cystamines **5**−**9** were synthesized using the carbodiimide−HOBt protocol,[35] using a convergent synthetic procedure to extend the peptide chain and to incorporate the redox-active ferrocene group, as summarized in Scheme 1. Boc−amino acid cystamines (**1** and **2**) were synthesized from the commercially available Boc-protected amino acids, Boc-Gly-OH and Boc-Ala-OH, and cystamine dihydrochloride in CH_2Cl_2 following established procedures.[33] The peptide chain of **2** was readily elongated by deprotection with TFA, followed the reaction with Boc-Ala-OH or Boc-Phe-OH to give compounds **3** and **4**, respectively. These peptide cystamines were the starting materials allowing the synthesis of the corresponding Fc−peptide cystamines **5**−**8** by an additional deprotection−coupling sequence, using ferrocene carboxylic acid as the acid component as previously described.[36] The unsymmetrical Fc−peptide cystamine **9** was obtained from a disulfide scrambling reaction of equimolar amounts of disulfides **2** and **3** followed by coupling with

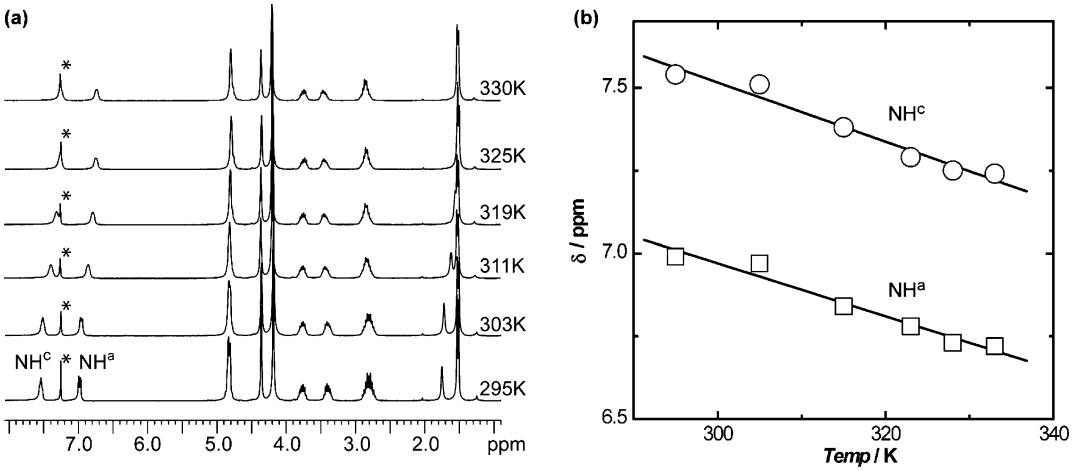

Figure 1. (a) ^{1}H NMR stack plots of **5** at 50 mM in $CDCl_3$ from 295 to 330 K. (b) The NH^a and NH^c amide protons shift upfield as temperature increases. An asterisk indicates residual $CHCl_3$.

CHART 1: Amide Proton Labeling Scheme Used for ^{1}H NMR Assignments

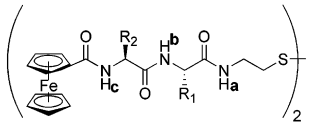

TABLE 2: Temperature Dependencies of the Chemical Shift of the Amide NH Protons at 1 and 50 mM in $CDCl_3$ for Compounds 5−9 Measured in ppb K^{-1} [a]

compound	NH^a 1 mM/50 mM	NH^b 1 mM/50 mM	NH^c 1 mM/50 mM
5	−5.9/−9.0		−6.0/−8.9
6	−6.8/−8.0		−6.7/−9.0
7	−10.3/−13.2	−9.9/−12.2	−11.0/−11.0
8	−6.2/−6.2	−8.1/−9.5	−11.6/−8.4
9	−4.1/−5.4	−5.6/−8.0	−8.0/−10.9

[a] See Scheme 2 for amide labeling.

two magnetically inequivalent ortho protons at δ 4.96−4.70 downfield from the signal for the meta protons at δ 4.50−4.22 and five protons for the unsubstituted Cp ring, which are observed close to δ 4.20 as observed for related compounds.[28,36,37,39,40]

Importantly, the ^{1}H NMR spectra of all compounds are very sensitive to temperature. Figure 1 shows a stack plot of ^{1}H NMR spectra of compound **6** recorded over a temperature range of 295−330 K at a concentration of 50 mM. The amide-labeling scheme use for the proton assignment is shown in Chart 1. Two major changes are noticeable as the temperature is increased.

First, the two amide resonances for the observed at δ 7.73 and at δ 7.01 shift upfield as the temperature is increased and experience peak broadening. The chemical shifts of the amide protons were plotted as a function of temperature giving linear relationships. The temperature dependences of the amide shifts for compounds **5**−**9** at two different concentrations are summarized in Table 2. Second, two peaks are observed for the methyl group of Ala at 295 K, which both merge into a single resonance at 319 K. We interpret these experimental findings as the result of intermolecular H-bonding between adjacent Fc−peptide cystamine molecules in solution. Both amide groups are involved in H-bonding and exhibit a typical temperature dependence (**5**, NH^a = −9.0 ppb K^{-1} and NH^c = −8.9 ppb K^{-1}; **6**, NH^a = −8.0 ppb K^{-1} and NH^c = −9.0 ppb K^{-1}) observed for interactions found in other Fc−peptide conjugates[37] and for unlabeled peptides.[41−43]

SCHEME 2: A Representation of the Multiple Equlibria in Solution that Compound 6 Can Adopt.

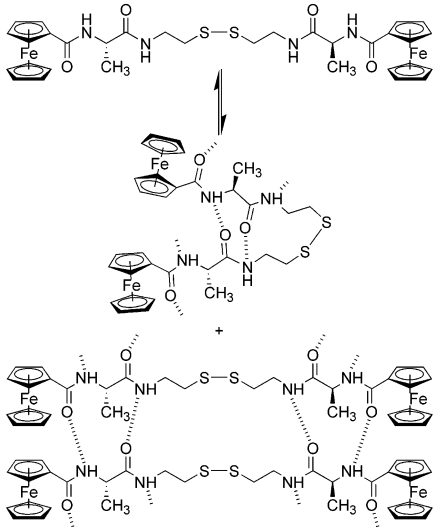

Note the intra- vs intermolecular H-bonding patterns that can each give rise to two populations of methyl groups for Ala.

It is clear that H-bonding in solution is a dynamic equilibrium. Thus, two potential molecular states will be present in solution, H-bonded and non-H-bonded molecules of compound **6** shown in Scheme 2. The methyl group of the Ala residue in **6** should give rise to two separate signals, one for the H-bonded and one for the non-H-bonded state. From the integration of the Ala CH_3 peaks, the ratio of the non-H-bonded to the H-bonded molecules is approximately 3:1, which gives an estimate of the association constant for a dimer of **6** at 295 K of $K_A > 200$ M^{-1}. Literature K_A values of related compounds for self-association of small peptides are in the range of 10−1000 M^{-1}.[42,44] Upon an increase in the temperature, the equilibrium is shifted more to the non-H-bonded state, consistent with the single resonance observed. Indeed, the two signals merge with a coalescence temperature of 319 K, allowing us to evaluate the thermodynamics of this process. An Eyring plot yields a $\Delta G^{\ddagger}_{298}$ of 70 kJ mol^{-1}, a $\Delta H^{\ddagger}$ of 90 kJ mol^{-1}, and a $\Delta S^{\ddagger}$ of 80 J K^{-1} mol^{-1} for this process. H-bonding was also assessed in solution by studying concentration effects by VT-NMR. At 1 mM concentrations, it is believed that intramolecular H-bonding will predominate and thus show strong amide shifts with temperature, whereas as 50 mM concentrations, H-bonding should be dominated by intermolecular interactions. The results

TABLE 3: FTIR Absorption Frequencies for the Amide Carbonyl and N−H Bands in a 6 mM Solution in $CHCl_3$ for Fc−Peptide Cystamines 5−9

compound	amide A (cm^{-1})	amide I (cm^{-1})
5	3412, 3314	1658, 1640
6	3420, 3315	1663, 1636
7	3420, 3315	1652, 1646
8	3407, 3326	1682, 1639
9	3424, 3320	1663, 1640

in Table 2 clearly show that all compounds studied exhibit H-bonding as indicated by the magnitude of the temperature dependencies on amide shift. Higher concentrations (50 mM) result in a greater amide upfield shift with temperature compared to the lower concentration (1 mM) amide shift, implying an intermolecular H-bonded system. However, at low concentrations (1 mM), the magnitude of the slope is consistent with intramolecular H-bonding. VT-NMR studies revealed that the compounds studied change the H-bonding pattern based on concentration.

Infrared results confirm the presence of H-bonding in solutions of compounds **5**−**9**. The amide group has potentially three modes, which may be sensitive toward H-bonding. In particular, the amide A and amide I bands are commonly used to investigate H-bonding.[45−47] The amide A band is highly sensitive and in many cases even shows the presence of H-bonded and non-H-bonded states. Absorptions for the amide A and amide I bands of compounds **5**−**9** in $CHCl_3$ solution are given in Table 3. The assignment of the carbonyl stretching absorptions for peptide and Fc−amide bands of compounds **5**−**9** is based on comparisons to related compounds, as described earlier.[19,26,37,48] Compounds **5**−**9** exhibited two signals in the amide I region, one of which falls into the narrow region of 1650−1635 cm^{-1}, which can be assigned to the Fc−CO stretch and the other one at slightly higher wavenumbers to the peptide−CO stretch.

However, it must be clearly stated that the amide I region is not suitable to distinguish and to assign H-bonded vs non H-bonded states since the expected shift of 10 cm^{-1} is expected to result in peak broadening. The amide A region, the region of the NH-stretching vibrations, on the other hand, often allows significant shifts of 100−200 cm^{-1} to lower frequencies for the H-bonded state.[49−54] All Fc−peptide cystamines investigated here exhibit two distinct absorption, as exemplified in Figure 2, which we assign to a H-bonded and a non-H-bonded state, in agreement with the ^{1}H NMR results.

The FTIR results of compound **6** in $CHCl_3$ are shown in Figure 2 at various concentrations. The two amide A stretches are at 3426 and 3321 cm^{-1} and correspond to the non-H-bonded and the H-bonded state, respectively. At higher concentrations (50 and 20 mM), the ratio of the peak areas is the same at 1:4. At lower concentrations, (6 and 1 mM) the ratio of the peak areas changes to 1:9. These results are corroborated with the ^{1}H NMR results, indicative of the dissociation of the intermolecular H bonds at low concentrations. However, our results do not rule out additional equilibria, as illustrated in Scheme 2, allowing for the formation of intramolecular H-bonded conformations.

We were fortunate to obtain single crystals for compounds **5** and **6**, which allow a more detailed analysis of the intermolecular H-bonding interactions that may resemble those in solution. The structure of the nonchiral Gly compound **5** was reported recently[33] and shows extensive intermolecular H-bonding resulting in the formation of a chiral supramolecular arrangement in which the two parts of the molecule are involved in the

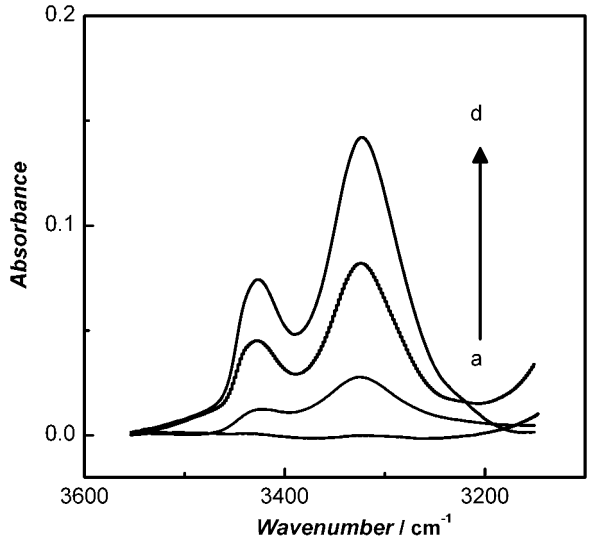

Figure 2. Amide A stretch of compound **6** in (a) 1 mM, (b) 6 mM, (c) 20 mM, and (d) 50 mM $CHCl_3$.

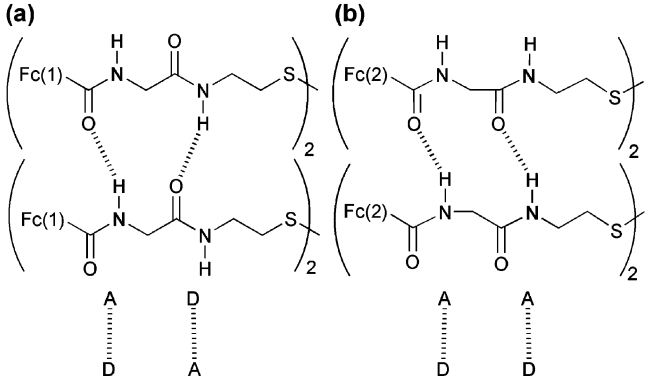

Figure 3. Two different H-bonding patterns (a) and (b) present in the solid state of **5**.

formation of two different H-bonding patterns illustrated in Figure 3. These results are in contrast to Hirao's work on 1,1′-disubstituted peptide ferrocenes, which exclusively exhibit intramolecular H-bonding leading to chiral patterning in the solid state.[26−28]

The Ala derivative **6** readily crystallizes from acetonitrile in the chiral space group $P2_1$, having two independent molecules per asymmetric unit. In addition, the asymmetric unit contains four molecules of acetonitrile. The ORTEP representation of **6** is shown in Figure 4a, together with selected bond distances and angles. Compound **6** exhibits features common to most monosubstituted ferrocenes and compares well to other Fc−peptides.[55] The Cp planes within the ferrocene groups are virtually coplanar and the Cp−Fe−Cp angle for all four Fc groups is in the range of 2.0−3.0° (Cp−Fe(1)−Cp = 2.8°, Cp−Fe(2)−Cp = 2.0°, Cp−Fe(3)−Cp = 2.8°, Cp−Fe(4)−Cp = 3.0°), which is typical for sterically unhindered systems. Similarly, the amide and Cp planes experience only a slight twist (amide/Cp twists: 18.7° for Fc(1), 7.2° for Fc(2), 16.0° for Fc(3), and 5.0° for Fc(4)), ensuring effective electronic communication between the ferrocene group and the podant peptide substituent. The S−S bond lengths within the cystamine subunit is 2.029(4) Å, which is similar to the corresponding Gly derivative, which has an S−S bond distance of 1.9879(11) Å. The two molecules adopt an extended conformation with dihedral angles of −104.7(5)° (C(16)−S(1)−S(2)−C(36)) and −99.2(5)° (C(56)−S(3)−S(4)−C(76)) about the two S−S

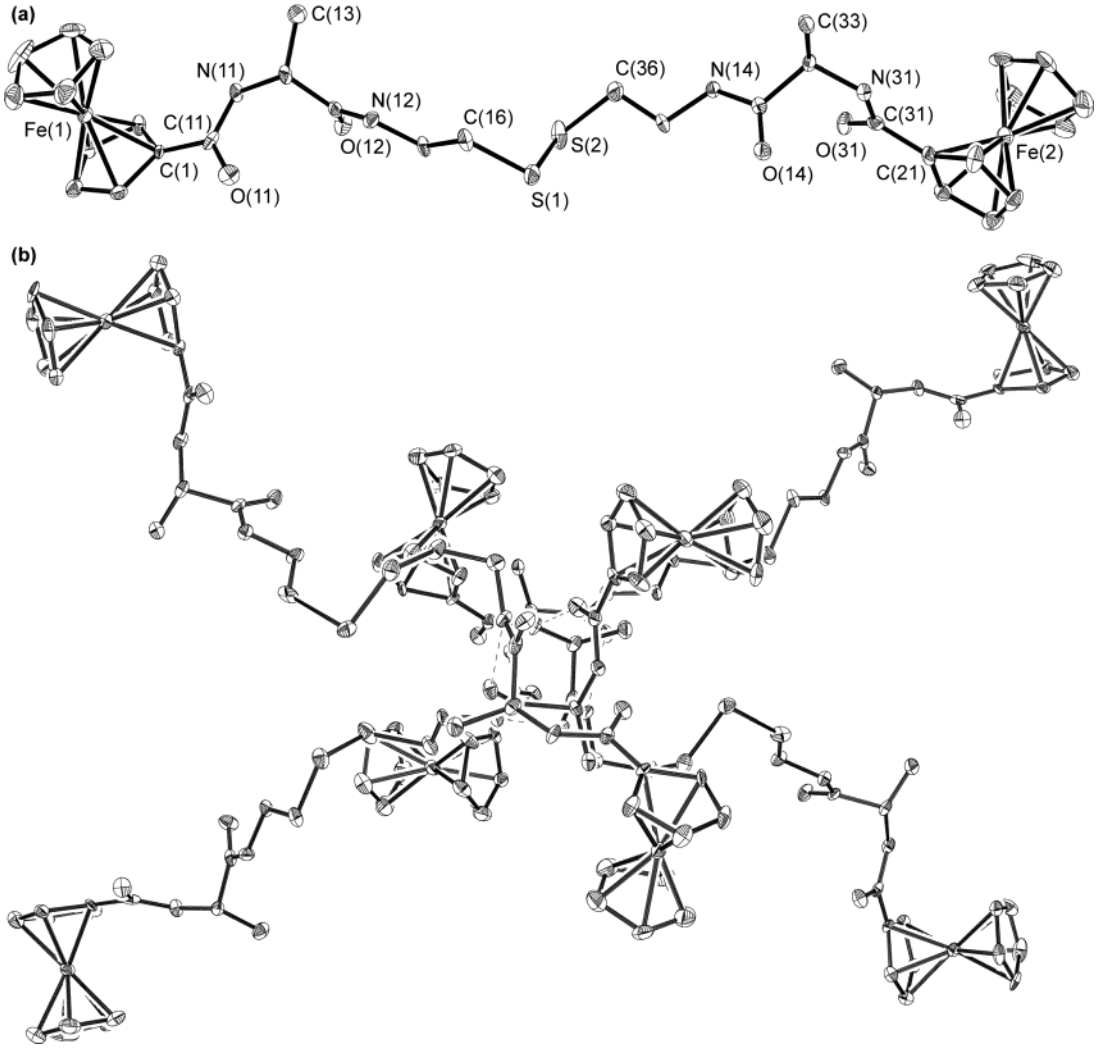

Figure 4. (a) ORTEP view of **6**. Selected bond angles and distances: d(C(1)−C(11)) = 1.500(12), d(C(21)−C(31)) = 1.461(12) Å, d(C(11)−O(11) = 1.232(11) Å, d(C(31)−O(31) = 1.219(12) Å, d(S(1)−S(2) = 2.029(4) Å. (b) Supramolecular network formed by intermolecular H-bonding between adjacent molecules of **6** resulting in the formation of a cystamine-linked network of β-helices. H-bond distances: d(O(21)−N(11)) = 2.804(10) Å, d(N(21)−O(11)) = 2.820(10) Å, d(O(22)−N(12)) = 2.971(11) Å, d(N(22)−O(12)) = 3.161(10) Å, d(O(24)−N(14)) = 2.884(9) Å, d(N(24)−O(14)) = 2.887(10) Å, d(O(23)−N(13)) = 3.053(10) Å, d(N(23)−O(13)) = 2.944(10) Å.

bonds. Importantly, this conformation enables the molecules to engage in extensive intermolecular H-bonding to it neighbors.

Compound **6** is held together by extensive intermolecular H bonds between the C═O and N−H groups of the Fc−amide and the Ala of compound **6**. Figure 4b shows the supramolecular network formed through intermolecular H-bonding in which each pair of the [Fc-Ala-CSA]$_2$ molecule participate in the formation of a left-handed β-helicate in which the H-bonding interaction resembles that of β-sheets. A closer inspection of the alanine residue of **6** reveals the dihedral angles to be ϕ = −72.3(4.7)°, ψ = 146.3(1.2)°, and ω = 173.4(3.2)°. These values compare well to a polypeptide adopting a polyproline II conformation where ideally the torsion angles are as follows: ϕ = −78°, ψ = 149°, and ω = 180°. Each Fc-labeled half of the molecule engages in H-bonding through the Fc−amide and cystamine with an identical portion of two neighboring molecules, one on each face, resulting in each molecule interacting with four adjacent molecules. Interestingly, the H-bonding pattern is different from that found in **5**, which contains two different H-bonding patterns. The Ala substitution apparently results in the loss of the "square helix". The structure of the monosubstituted Fc-Ala-ProOEt also forms an extended intermolecular H-bonded network through its alanine amide residue.[27] The amide/Cp twist in Fc-Ala-ProOEt is approximately 24°, which is slightly larger than that observed in **6**. The incorporation of an additional H-bonding moiety in Fc-Ala-Pro-NHPy leads to a H-bonded network that results in an amide/Cp twist of only 3.7°. This suggests that enhancing the H-bonded network will restrict movement of the Fc groups and force the Cp ring to be coplanar with the attached amide resulting in enhanced electronic communication.

(b) Electrochemical Studies. *Solution Electrochemistry.* As part of our characterization of compounds **5**−**9**, we explored their solution electrochemistry by cyclic voltammetry using conventional glassy carbon electrodes (BAS 3.0-mm diameter). Figure 5 shows a typical CV of compound **5**. All systems exhibit a reversible one-electron oxidation (see Table 4). The peak separation (ΔE_p) between the oxidation and reduction peaks was between 66 and 73 mV for all the systems investigated. The ratio of anodic to cathodic peak currents were close to unity.[56,57] Interestingly, the Fc half-wave potentials ($E_{1/2}$) are virtually insensitive to the peptide substituent and are within the range of 586−601 mV, showing a linear relationship between anodic peak currents and square root of the scan rate, typical for diffusion controlled processes.[58] However, aliquots of H_2O added to the electrochemical solution had a dramatic effect on the $E_{1/2}$ values which changed to 450 mV when the mole ratio was 1:9 (CH_3CN-H_2O), just before precipitation of the Fc

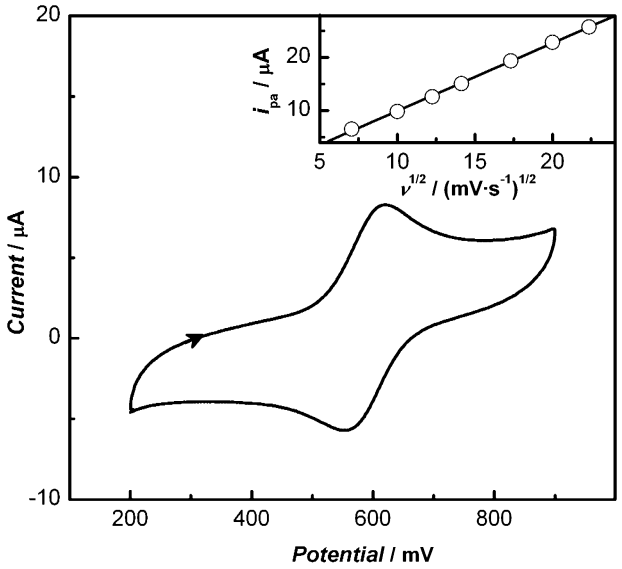

Figure 5. CV for 1 mM of compound **6** in 0.1 M TBAP/CH_3CN from a potential of 100−800 mV at a scan rate of 100 mV s^{-1} vs Ag/AgCl. Inset: linear relationship between square root of the scan rate and anodic peak current.

TABLE 4: Electrochemical Results of Compounds 5−9 in CH_3CN Solution. Glassy Carbon Working Electrode, Pt Counter, Ag/AgCl Reference, 0.1 M TBAP[a]

compound	$E_{1/2}$ (mV)	ΔE_p (mV)	i_{pa}/i_{pc}
5	596 (6)	66 (3)	1.06
6	587 (7)	67 (2)	1.06
7	593 (4)	73 (3)	1.04
8	586 (5)	68 (2)	1.11
9	601 (5)	70 (4)	1.09

[a] Standard deviations are in parentheses.

peptide. Half-wave potentials generally correspond well with earlier reports on related systems.[19,37,59−62] As learned from the solution NMR and IR spectroscopic studies, all systems studied here exhibit H-bonding interactions, especially at high concentrations (vide supra). Importantly, any supramolecular structure adopted in solution appears to have little effect on the half-wave potential of the compounds. This compares well to the results of the visible spectroscopy, in which all Fc systems exhibit concentration independent single broad absorption with an absorption maxima at λ_{max} at 442(2) nm and with molar absorptivities in the range of $200 < \epsilon < 550$ M^{-1} cm^{-1}.

Monolayer Studies. All monolayer studies were carried out on 50-μm gold microelectrodes. Fc−peptide cystamines are convenient starting materials for the preparation of Fc−peptide cystamine monolayers on gold.[19] Self-assembled monolayers (SAMs) can readily be prepared from molecules containing thiols, disulfides, and sulfides on common metal substrates such as gold, platinum, and mercury.[63−67] Our general approach, using disulfide **5**, for SAM preparation on a Au surface is shown in Figure 6. As expected, the capacitive background current drops after attachment of the Fc−peptides to the surface to about 75% of that of the bare Au surface. Little variation in capacitive current was observed for monolayers of **5**−**9**, suggesting further evidence for a loosely packed monolayer.

A typical CV curve of the monolayer of compound **5** on gold is shown in Figure 6. Other Fc−peptides gave similar results. From the background-subtracted CVs, the Coulombic charge was obtained by integration, which allows the determination of the surface coverage and the specific area occupied by each molecule, summarized in Table 5. All coverage values fall

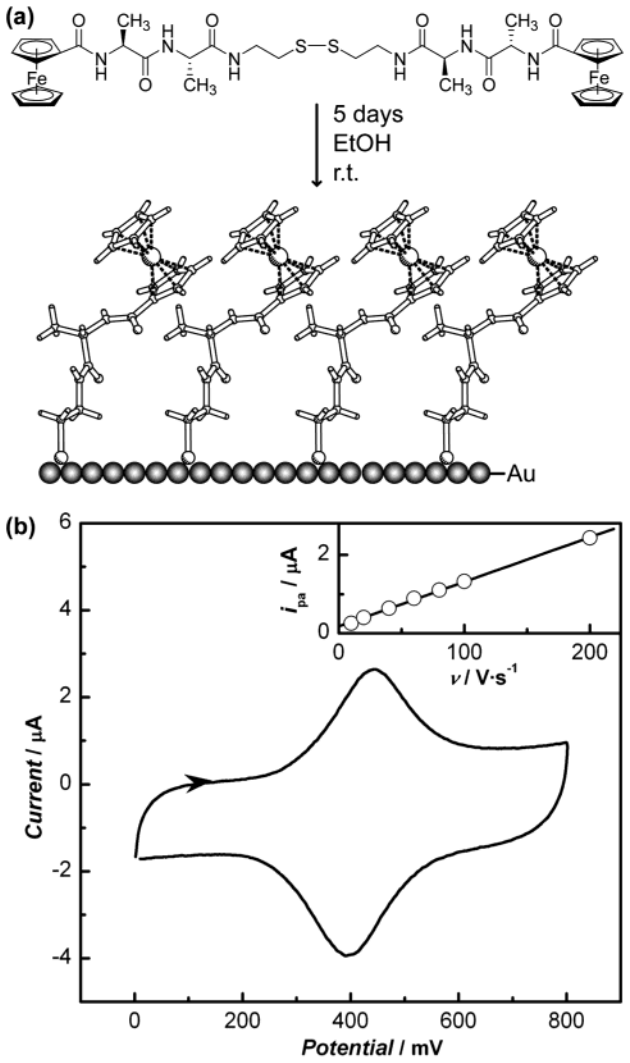

Figure 6. (a) Monolayer formation of **5** on gold. (b) Cyclic voltammogram of a gold microelectrode (50 μm diameter), modified with **7** in 2 M $NaClO_4$ (aq). The arrow indicates the rest potential and thus, the starting potential. Scan rate of 200 V s^{-1}, Pt counter, Ag/AgCl reference. Inset: linear relationship between scan rate and peak current.

TABLE 5: Surface Properties of Fc−Peptide SAMs for Compounds 5−9 on Au Microelectrodes (50 μM)[a]

compound	Γ_{max} (molecules cm^{-2})	Cu UPD	specific area (Å^2 molecule^{-1})	thickness (Å)
bare Au		3.00×10^{10}		
5	3.7×10^{13}	5.17×10^{9}	270	7(1)
6	3.4×10^{13}	4.49×10^{9}	290	6(1)
7	3.0×10^{13}	5.46×10^{9}	330	9(1)
8	3.0×10^{13}	4.24×10^{9}	330	9(1)
9	3.2×10^{13}	5.63×10^{9}	310	8(2)
6 + **7**	3.1×10^{13}		320	9(2)

[a] Standard deviations are in parentheses.

within the range of $(4-3) \times 10^{13}$ molecules cm^{-2}, which are approximately one-tenth less than the maximum theoretical coverage of $(1-4) \times 10^{14}$ molecules cm^2 calculated for a monolayer of ferrocenoyl alkanethiols on Au(111).[68−70] Thus, coverages are reasonable considering the Fc−peptide cystamines are bulkier than nonbranched ferrocenoyl alkanethiols. However, we must also consider the presence of defect or pinholes within the monolayer structure. Specific areas found for compounds **5**−**9** fall within the range of 270−330 Å^2, which is somewhat greater than that for Fc−oligoprolines (180−240 Å^2 molecule)[19]

TABLE 6: Electrochemical Properties of Hexanethiol-Diluted and -Undiluted Fc−Peptide Cystamine SAMs on Gold Microelectrodes[a]

	undiluted SAMs				diluted SAMs			
compound	$E^{0\prime}$ (mV)	ΔE_p (mV)	i_{pa}/i_{pc}	ΔE_{fwhm} (mV)	$E^{0\prime}$ (mV)	ΔE_p (mV)	i_{pa}/i_{pc}	ΔE_{fwhm} (mV)
5	485 (8)	28 (10)	1.1	113 (8)	511 (11)	11 (5)	1.1	100 (10)
6	472 (6)	44 (10)	1.1	116 (15)	505 (13)	11 (5)	1.1	110 (12)
7	461 (15)	15 (9)	1.1	116 (10)	488 (10)	33 (12)	1.0	122 (15)
8	510 (10)	22 (8)	1.0	128 (14)	524 (15)	16 (7)	1.0	122 (11)
9	499 (9)	74 (11)	1.1	180 (25)	521 (17)	44 (9)	0.9	133 (12)
6 + 7	479 (15)	70 (15)	1.1	180 (29)	517 (11)	60 (10)	0.9	153 (14)

[a] 2.0 M of $NaClO_4$ (aq), scan rate of 10 V s^{-1}, Pt counter electrode, potential vs Ag/AgCl. Standard deviations are in parentheses.

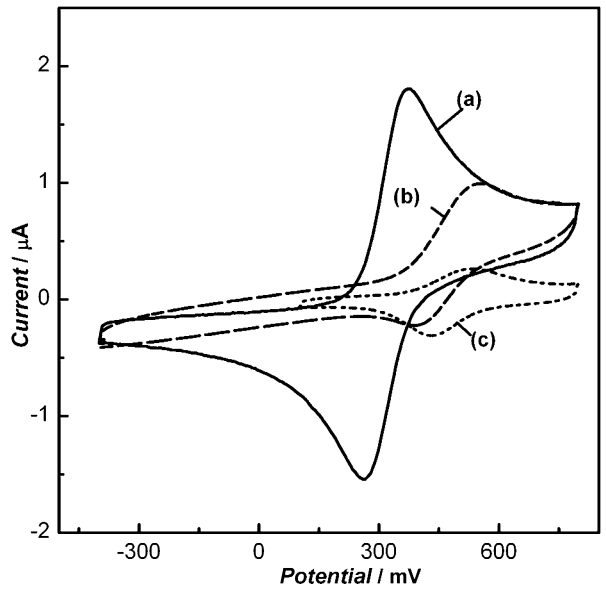

Figure 7. CVs for (a) bare gold microelectrode (50 μm) with 10 mM $[Fe(CN)_6]^{3-/4-}$ in 2.0 M $NaClO_4$(aq), (b) **5**-modified electrode with 10 mM $[Fe(CN)_6]^{3-/4-}$ in 2.0 M $NaClO_4$(aq), (c) **5**-modified electrode in 2.0 M $NaClO_4$(aq) at a scan rate of 20 V s^{-1} and a Ag/AgCl reference electrode.

but compares well with the specific areas of other peptide.[71] Others, using fluorescent techniques, found the area occupied by fluorescent-labeled helical peptides varied from 280 to 420 Å^2.[72,73] The higher space requirements found for **5**−**9** compared to oligoprolines are presumably due to a loose packing of these nonhelical peptides. Monolayer thickness was determined by ellipsometry and all values are between 6(1) and 9(1) Å, which compares well with the molecular dimensions of compounds **5**−**9**. The thickness measurements are used to confirm the presence of a monolayer and a lack of multilayer structures.

Thus, it is expected that the Fc−peptide SAMs are in effect nonideal and may be "leaky". UPD of Cu experiments were carried out to determine the amount of Au still exposed to the bulk solution after monolayer preparation. The amount of Cu that was deposited after monolayer formation indicated that between 15 and 20% of the Au surface was unprotected and little variation between monolayers was observed.

Blocking studies were carried out on the modified Au electrodes using the $[Fe(CN)_6]^{3-/4-}$ redox couple in solution to assess the effectiveness of the Fc−peptides blocking access of the solution electrophore to the Au surface. The blocking studies, shown in Figure 7, show an attenuation of the $[Fe(CN)_6]^{3-/4-}$ redox probe signal due to limited access to the Au surface (compare CV of part a with part b of Figure 7). Incomplete blockage is expected because the Cu UPD experiments clearly indicate that exposed Au remains after 5 days of incubation. However, the CV of Figure 7b shows an $E_{1/2}$ of 485 mV, which corresponds to Fc/Fc^+, not $[Fe(CN)_6]^{3-/4-}$. Figure 7c is included to show the $E^{0\prime}$ of Fc/Fc^+ in the absence of a solution-based redox probe. Interestingly, a large enhancement of the peak current is observed in Figure 7b compared to Figure 7c. Similar communication between an electroactive monolayer and a solution electrophore were observed by Creager[74,75] for Fc−alkylthiol systems. The observations are rationalized by an ET cycle where one Fc^+ can be reduced by $[Fe(CN)_6]^{4-}$ in close proximity, allowing for another oxidation of the Fc within the one oxidative CV cycle. This cycle can occur several times because of the ample amount of sacrificial solution-based electrophore. A reviewer pointed out that the i_{pa} is much larger than the i_{pc} in Figure 7b, which is due to the different rates of the ferrocenium-mediated ferrocyanide oxidation (faster and larger peak) and the ferrocene-mediated ferricyande reduction (slower and smaller peak). The oxidation is faster than the reduction because the ferrocene potential is positive of the ferrocyanide redox potential. We assume that due to the electronic interactions possible in peptides[19,76−78] that communications through the peptide spacer facilitates "through-monolayer" ET to the electrophore.

Gold microelectrodes are particularly useful for the determination of the ET kinetics in peptide SAMs.[79,80] Figure 6b shows the CV of a 50-μm gold electrode modified with compound **5** in 2 M $NaClO_4$. We chose a high ionic strength in order to reduce the solution resistance and thus minimize the *iR* drop. Like in solution, all systems exhibit a fully reversible one-electron oxidation of the Fc moiety. However, on the surface, the ET is no longer diffusion controlled but a function of the spacer between the electrophore and the transducer surface. Table 6 summarizes the results of the CV experiments for undiluted and hexanthiol-diluted monolayers of Fc−peptides. Previous results have shown that the redox potential of the ferrocenoyl group can be sensitive to the attached substituent.[19,40] In these short Fc−peptide systems, small variations were observed, which is in line with others.[76−78]

Figure 6b shows a CV for compound **5** attached to a gold microelectrode at a scan rate of 200 V s^{-1}. The redox behavior of all systems is reversible as judged from the ratio of the peak currents. The inset of Figure 6b demonstrates successful immobilization of the ferrocenoyl oligopeptide disulfide on the gold surface.[81−84] Furthermore, monolayers of compound **5**−**9** were studied after surface dilution with hexanethiol. The nonredox-active diluent has the effect of isolating the Fc units from lateral electron transfer as indicated by the general decrease in ΔE_{fwhm} value toward an ideal of 90 mV.[85] The hexanethiol will also fill defect sites and form a more rigid system due to tighter packing of the unbranched alkyl chains. The $E^{0\prime}$ values for the SAMs of compounds **5**−**9** are similar and show no unique structural trends. However, the addition of a diluent causes the $E^{0\prime}$ value to shift anodically, which is consistent with the Fc moiety in a more hydrophobic surrounding.[86] The CVs for SAMs of compound **9** and the mixed **6** + **7** showed a large ΔE_{fwhm}, suggesting large disorder among the Fc groups. The

TABLE 7: Electrochemical Properties of the Hexanethiol Diluted Fc−Peptide Cystamine SAMs on Gold Microelectrodes[a]

	undiluted monolayers		diluted monolayers	
compound	k_{ET} (10^3 s^{-1})	α	k_{ET} (10^3 s^{-1})	α
5	7.0 (1)	0.5	7.1 (1)	0.5
6	5.1 (1)	0.5	5.3 (1)	0.5
7	5.3 (1)	0.5	7.8 (1)	0.4
8	4.4 (1)	0.5	5.6 (1)	0.5
9	4.2 (1)	0.5	6.5 (1)	0.4
6 + **7**	4.3 (1)	0.5	7.2 (1)	0.4

[a] 2.0 M of $NaClO_4$ (aq), scan rate of 1000 V s^{-1}, Pt counter electrode, potential vs Ag/AgCl. Calculated ET rate constants for compounds **5**−**9** using Butler−Volmer formalism (see Supporting Information for details). Standard deviations are in parentheses.

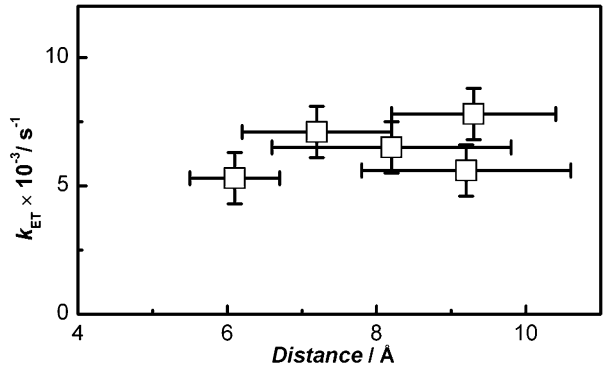

Figure 8. Relationship between ET rates and donor−acceptor distances in Å for hexanethiol-diluted SAMs of compounds **5**−**9** (see Supporting Information for undiluted SAMs). Error bars indicate standard deviations in k_{ET} and thickness measurements.

amount of disorder was reduced upon hexanethiol monolayer dilution, but the ΔE_{fwhm} of **9** and the mixed **6** + **7** still remained the highest of the compounds studied. The separation between oxidation and reduction peaks, ΔE_p, for ideal redox-active monolayers is 0 mV and all compounds examined were in the range of 11−70 mV. The anodic−cathodic peak ratio is close to unity for all compounds, supporting reversibility.

ET rates were obtained from the CVs by the Butler−Volmer formalism and the results are shown in Table 7.[58] Murray and Creager reported on the use of CV to evaluate ET rate constants in Fc-labeled alkanethiol monolayers.[87,88] The use of fast scan rates, which is required for heterogeneous rate constant determination in our system, can lead to large errors due to *iR* drop. Fortunately, the solution resistance was small (2−5 Ω cm^2), as measured by impedance spectroscopy and has little effect even at the highest scan rate (1000 V s^{-1}) where currents are 20−30 μA. As shown in Table 7, the addition of the monolayer diluent causes a slight increase in k_{ET}. The enhanced rate is likely caused by "stiffening" of the monolayer. Generally, ET rates decreased slightly as the chain length increases.[19,89−93] According to Marcus theory,[89] an increase in distance between the electrode surface and the Fc group should result in a decrease of the k_{ET} by 1 order of magnitude per 2.3 Å.

The distance dependence, as measured by ellipsometry, on k_{ET} is shown in Figure 8 for compounds **5**−**9**. A system involving monolayers of $Fc-CONH(CH_2)_nSH$ was studied[91] using CV, and the k_{ET} values found were 6.6×10^4, 1.5×10^4, 6.0×10^3, 1.2×10^3, and 6.6 s^{-1}, where $n = 7-10$ and 15, respectively. Another related study compared k_{ET} values of two similar compounds, $Fc-(CH_2)_8SH$ and $Fc-CO_2(CH_2)_8SH$, using CV.[94] The results provided k_{ET} values of 4.1×10^3 and 4.5×10^4 s^{-1} for the Fc alkanethiol and the Fc ester, respectively. The magnitude of the rate constants in our peptidic systems is a factor of 10 lower, which is rationalized by the poorly packed monolayers shown by Cu UPD experiments above. A comparison of **5** and **6** reveals that the additional bulk of an extra methyl group of alanine leads to a slightly lower ET rate. This could be explained by the less rigid system, as the additional methyl group of alanine may not allow for as tight packing as the glycine system. There is no difference in ET rates of the Fc-Ala (**6**) and the Fc-Ala-Ala (**7**) systems, which implies that distance to the electrophore has little effect on ET rate for peptidic systems. The lack of a distance dependence could be explained by efficient through-bond electronic coupling of the Fc through the peptide spacer to the Au surface. Alternatively, the large amount of disorder within these short peptidic chains allows the Fc group to be positioned at approximately the same distance from the electrode surface in all of the monolayers studied. The ET rates observed are all very similar and can be correlated to the thickness of the peptides on the surface. All of the compounds tested have approximately the same thickness and the similar ET rates, thus little insight to the structural effects on ET rate is gained. Furthermore, the electron-transfer rates have no correlation to the linker structure, indicating that R groups of amino acids do not play an electronic role in these systems. It is possible that the N−C−C− peptide backbone permits efficient through-bond ET and the R group of the amino acids chosen behave purely in a monolayer-packing motif. Although, the effects of packing are negligible in such short peptide sequences and longer peptides are needed to probe this issue.

Summary and Future Work

In conclusion, we have synthesized and fully characterized a series of Fc−peptide cystamines. Crystal structures of the **5** and **6** show extensive intermolecular H-bonded networks creating β-helicate supramolecular structures. These results differ significantly from Hirao's work on disubstituted 1,1′-Fc−peptide systems which exhibit exclusively intramoleular H-bonding interactions, leading to chiral patterning in the solid state. Solution VT ^1H NMR and FTIR results confirmed the presence of H-bonding interactions. Solution electrochemical studies were carried out in CH_3CN and showed only minor variation between compounds **5**−**9**. In general, on the surface, the molecules do not pack tightly and leave about 15−20% of the surface accessible, with the result that the monolayers of compounds **5**−**9** are not well ordered and leaky. The kinetics of ET were estimated using the Butler−Volmer formalism and are in the range of $[5(1)-8(1)] \times 10^3$ s^{-1}. Monolayer dilution studies with hexanethiol have shown that a more rigid monolayer undergoes faster redox kinetics and that the change in the k_{ET} value is more pronounced in the longer peptides. Future work will look at longer sequences that adopt a defined secondary structure to probe ET and secondary structure effects.

Acknowledgment. The authors thank the Natural Sciences and Engineering Research Council for funding. We also wish to thank Bob McDonald, University of Alberta, for the data collection of compounds **5** and **6**. H.B.K. is the Canada Research Chair in Biomaterials.

Supporting Information Available: Cu UPD results, absorbance maxima and molar absorptivities, ^1H and $^{13}C\{H\}$ NMR chemical shift and coupling constants, sonication effects on monolayer coverage, water solvent effects on $E_{1/2}$ of **5** and **6** in CH_3CN, packing diagram of **6**, an Eyring plot of **5**, and ET rate calculations method. This material is available free of charge via the Internet at http://pubs.acs.org.

References and Notes

(1) Isied, S. S.; Ogawa, M. Y.; Wishart, J. F. *Chem. Rev.* **1992**, *92*, 381−390.

(2) Bobrowski, K.; Poznanski, J.; Holcman, J.; Wierzchowski, K. L. *J. Phys. Chem. B* **1999**, *103*, 10316−10324.

(3) Bobrowski, K.; Holcman, J.; Poznanski, J.; Wierzchowski, K. L. *Biophys. Chem.* **1997**, *63*, 153−166.

(4) Isied, S. S.; Moreira, I.; Ogawa, M. Y.; Vassilian, A.; Arbo, B.; Sun, J. *J. Photochem. Photobiol. A* **1994**, *82*, 203−210.

(5) Mishra, A. K.; Chandrasekar, R.; Faraggi, M.; Klapper, M. H. *J. Am. Chem. Soc.* **1994**, *116*, 1414−1422.

(6) Ogawa, M. Y.; Moreira, I.; Wishart, J. F.; Isied, S. S. *Chem. Phys.* **1993**, *176*, 589−600.

(7) Ogawa, M. Y.; Wishart, J. F.; Young, Z. Y.; Miller, J. R.; Isied, S. S. *J. Phys. Chem.* **1993**, *97*, 11456−11463.

(8) Bobrowski, K.; Holcman, J.; Poznanski, J.; Ciurak, M.; Wierzchowski, K. L. *J. Phys. Chem.* **1992**, *96*, 10036−10043.

(9) Li, J.; Schuler, K.; Creager, S. E. *J. Electrochem. Soc.* **2000**, *147*, 4584−4588.

(10) Brevnov, D. A.; Finklea, H. O. *J. Electrochem. Soc.* **2000**, *147*, 3461−3466.

(11) Ohtani, M. *Electrochem. Commun.* **1999**, *1*, 488−492.

(12) Creager, S. E.; Wooster, T. T. *Anal. Chem.* **1998**, *70*, 4257−4263.

(13) Andreu, R.; Calvente, J. J.; Fawcett, W. R.; Molero, M. *Langmuir* **1997**, *13*, 5189−5196.

(14) Ohtani, M.; Kuwabata, S.; Yoneyama, H. *Anal. Chem.* **1997**, *69*, 1045−1053.

(15) Doron, A.; Portnoy, M.; Lion-Dagan, M.; Katz, E.; Willner, I. *J. Am. Chem. Soc.* **1996**, *118*, 8937−8944.

(16) Creager, S. E.; Weber, K. *Langmuir* **1993**, *9*, 844−850.

(17) Chidsey, C. E. D.; Bertozzi, C. R.; Putvinski, T. M.; Mujsce, A. M. *J. Am. Chem. Soc.* **1990**, *112*, 4301−4306.

(18) Yeo, W. S.; Hodneland, C. D.; Mrksich, M. *ChemBioChem* **2001**, *2*, 590−593.

(19) Galka, M. M.; Kraatz, H.-B. *ChemPhysChem* **2002**, *3*, 356−359.

(20) Karle, I. L.; Ranganathan, D.; Haridas, V. *J. Am. Chem. Soc.* **1996**, *118*, 10916−10917.

(21) Karle, I. L.; Ranganathan, D.; Lakshmi, C. *Biopolymers* **2001**, *59*, 301−304.

(22) Ranganathan, D.; Haridas, V.; Nagaraj, R.; Karle, I. L. *J. Org. Chem.* **2000**, *65*, 4415−4422.

(23) Ranganathan, D.; Haridas, V.; Sundari, C. S.; Balasubramanian, D.; Madhusudanan, K. P.; Roy, R.; Karle, I. L. *J. Org. Chem.* **1999**, *64*, 9230−9240.

(24) Ranganathan, D.; Lakshmi, C.; Karle, I. L. *J. Am. Chem. Soc.* **1999**, *121*, 6103−6107.

(25) Ranganathan, D.; Haridas, V.; Karle, I. L. *J. Am. Chem. Soc.* **1998**, *120*, 2695−2702.

(26) Moriuchi, T.; Nomoto, A.; Yoshida, K.; Ogawa, A.; Hirao, T. *J. Am. Chem. Soc.* **2001**, *123*, 68−75.

(27) Nomoto, A.; Moriuchi, T.; Yamazaki, S.; Ogawa, A.; Hirao, T. *Chem. Commun.* **1998**, 1963−1964.

(28) Moriuchi, T.; Nomoto, A.; Yoshida, K.; Hirao, T. *J. Organomet. Chem.* **1999**, *589*, 50−58.

(29) Moriuchi, T.; Hirao, T. *J. Synth. Org. Chem. Jpn.* **2001**, *59*, 1195−1203.

(30) Moriuchi, T.; Yoshida, K.; Hirao, T. *J. Organomet. Chem.* **2001**, *637*, 75−79.

(31) Moriuchi, T.; Yoshida, K.; Hirao, T. *Organometallics* **2001**, *20*, 3101−3105.

(32) Moriuchi, T.; Nomoto, A.; Yoshida, K.; Hirao, T. *Organometallics* **2001**, *20*, 1008−1013.

(33) Bediako-Amoa, I.; Silerova, R.; Kraatz, H.-B. *Chem. Commun.* **2002**, 2430−2431.

(34) Baranski, A.; Szulborska, A. *J. Electroanal. Chem.* **1994**, *373*, 157−165.

(35) Bodansky, M.; Bodansky, A. *The Practise of Peptide Synthesis*; Springer-Verlag: Berlin, 1984.

(36) Kraatz, H. B.; Lusztyk, J.; Enright, G. D. *Inorg. Chem.* **1997**, *36*, 2400−2405.

(37) Saweczko, P.; Enright, G. D.; Kraatz, H. B. *Inorg. Chem.* **2001**, *40*, 4409−4419.

(38) Saweczko, P.; Kraatz, H. B. *Coord. Chem. Rev.* **1999**, *192*, 185−198.

(39) Zhang, L.; Godinez, L. A.; Lu, T.; Gokel, G. W.; Kaifer, A. E. *Angew. Chem., Int. Edit. Engl.* **1995**, *235*, 327−335.

(40) Kraatz, H. B.; Leek, D. M.; Houmam, A.; Enright, G. D.; Lusztyk, J.; Wayner, D. D. M. *J. Organomet. Chem.* **1999**, *589*, 38−49.

(41) Gellman, H. S.; Adams, B. R. *Tetrahedron Lett.* **1989**, *30*, 3381−3384.

(42) Kirsten, C. N.; Schrader, T. H. *J. Am. Chem. Soc.* **1997**, *119*, 12061−12068.

(43) Nowick, J. S.; Mahrus, S.; Smith, E. M.; Ziller, J. W. *J. Am. Chem. Soc.* **1996**, *118*, 1066−1072.

(44) Wehner, M.; Schrader, T. *Angew. Chem., Int. Edit.* **2002**, *41*, 1751−1754.

(45) Chehin, R.; Iloro, I.; Marcos, M. J.; Villar, E.; Shnyrov, V. L.; Arrondo, J. L. R. *Biochemistry* **1999**, *38*, 1525−1530.

(46) Dong, A.; Matsura, J.; Manning, M. C.; Carpenter, J. F. *Arch. Biochem. Biophys.* **1998**, *355*, 275−281.

(47) Jackson, M.; Mantsch, H. H. *Crit. Rev. Biochem. Mol. Biol.* **1995**, *30*, 95−120.

(48) Huang, R.; Wang, Q. *J. Organomet. Chem.* **2001**, *637*, 94−98.

(49) Miyazawa, T.; Blout, E. R. *J. Am. Chem. Soc.* **1961**, *83*, 712−719.

(50) Brauner, J. W.; Dugan, C.; Mendelsohn, R. *J. Am. Chem. Soc.* **2000**, *122*, 677−683.

(51) Tonan, K.; Ikawa, S.-i. *J. Am. Chem. Soc.* **1996**, *118*, 6960−6965.

(52) Gu, Z.; Zambrano, R.; McDermott, A. *J. Am. Chem. Soc.* **1994**, *116*, 6368−6372.

(53) Tor, Y.; Libman, J.; Shanzer, A.; Felder, C. E.; Lifson, S. *J. Am. Chem. Soc.* **1992**, *114*, 6653−6661.

(54) Toniolo, C.; Bonora, G. M.; Marchiori, F.; Borin, G. *J. Am. Chem. Soc.* **1984**, *106*, 1455−1457.

(55) Lin, L.; Berces, A.; Kraatz, H. B. *J. Organomet. Chem.* **1998**, *556*, 11−20.

(56) Kissinger, P. T. *J. Chem. Educ.* **1983**, *60*, 702−706.

(57) Gomez, M. E.; Kaifer, A. E. *J. Chem. Educ.* **1992**, *69*, 502−505.

(58) Bard, A. J.; Faulkner, L. R. *Electrochemical Methods*, 2nd ed.; John Wiley and Sons: New York, 2001.

(59) Di Gleria, K.; Hill, H. A. O.; Wong, L. L. *FEBS Lett.* **1996**, *390*, 142−144.

(60) Hess, A.; Sehnert, J.; Weyhermueller, T.; Metzler-Nolte, N. *Inorg. Chem.* **2000**, *39*, 5437−5443.

(61) Xu, Y.; Saweczko, P.; Kraatz, H.-B. *J. Organomet. Chem.* **2001**, *637*−*639*, 335−342.

(62) Kraatz, H.-B.; Leek, D. M.; Houmam, A.; Enright, G. D.; Lusztyk, J.; Wayner, D. D. M. *J. Organomet. Chem.* **1999**, *589*, 38−49.

(63) Finklea, H. O.; Ravenscroft, M. S.; Snider, D. A. *Langmuir* **1993**, *9*, 223−227.

(64) Finklea, H. O.; Hanshew, D. D. *J. Am. Chem. Soc.* **1992**, *114*, 3173−3181.

(65) Chidsey, C. E. D. *Science* **1991**, *252*, 631−631.

(66) Becka, A. M.; Miller, C. J. *J. Phys. Chem.* **1992**, *96*, 2657−2668.

(67) Ulman, A. *Chem. Rev.* **1996**, *96*, 1533−1540.

(68) Viana, A. S.; Abrantes, L. M.; Jin, G.; Floate, S.; Nichols, R. J.; Kalaji, M. *Phys. Chem. Chem. Phys.* **2001**, *3*, 3411−3419.

(69) Whitesides, G. A.; Folkers, J. P.; Laibinis, P. E. *Langmuir* **1992**, *8*, 1330−1336.

(70) Whitesides, G. M.; Laibinis, P. E. *Langmuir* **1990**, *6*, 87−96.

(71) Sakamoto, S.; Aoyagi, H.; Mihara, H.; Nakashima, N. *J. Chem. Soc. Perkin Trans. 2* **1996**, 2319−2324.

(72) Hossain, M. A.; Hamasaki, K.; Takahashi, K.; Mihara, H.; Ueno, A. *J. Am. Chem. Soc.* **2001**, *123*, 7435−7436.

(73) Obataya, I.; Sakamoto, S.; Ueno, A.; Mihara, H. *Biopolymers* **2001**, *59*, 65−71.

(74) Radford, T. R.; Creager, S. E. *Anal. Chim. Acta* **2001**, *449*, 199−209.

(75) Radford, T. R.; French, M.; Creager, S. E. *Anal. Chem.* **1999**, *71*, 5101−5108.

(76) Antonello, S.; Formaggio, F.; Moretto, A.; Toniolo, C.; Maran, F. *J. Am. Chem. Soc.* **2003**, *125*, 2874−2875.

(77) Antonello, S.; Crisma, M.; Formaggio, F.; Moretto, A.; Taddei, F.; Toniolo, C.; Maran, F. *J. Am. Chem. Soc.* **2002**, *124*, 11503−11513.

(78) Antonello, S.; Benassi, R.; Gavioli, G.; Taddei, F.; Maran, F. *J. Am. Chem. Soc.* **2002**, *124*, 7529−7538.

(79) Ching, S.; Dudek, R.; Tabet, E. *J. Chem. Educ.* **1994**, *71*, 602−605.

(80) Stulik, K.; Amatore, C.; Holub, K.; Marecek, V.; Kutner, W. *Pure Appl. Chem.* **2000**, *72*, 1483−1492.

(81) Wang, J. B. *Analytical Elecrochemistry*, 2nd ed.; John Wiley and Sons: New York, 2000.

(82) Greef, R.; Peat, R.; Peter, L. M.; Pletcher, D.; Robinson, J. *Instrumental Methods in Electrochemistry*; John Wiley and Sons: New York, 1985.

(83) Finklea, H. O.; Hanshew, D. D. *J. Electroanal. Chem.* **1993**, *347*, 327−340.

(84) Campbell, D. J.; Herr, B. R.; Hulteen, J. C.; Van Duyne, R. P.; Mirkin, C. A. *J. Am. Chem. Soc.* **1996**, *118*, 10211−10219.

(85) Finklea, H. O. *Electroanalytical Chemistry*; Marcel Dekker: New York, 1996; Vol. 19.

(86) Baker, M. V.; Kraatz, H. B.; Quail, J. W. *New J. Chem.* **2001**, *25*, 427−433.

(87) Creager, S. E.; Rowe, G. K. *J. Electroanal. Chem.* **1994**, *370*, 203−211.

(88) Tender, L.; Carter, M. T.; Murray, R. W. *Anal. Chem.* **1994**, *66*, 3173−3181.

(89) Marcus, R. A. *J. Phys. Chem.* **1992**, *96*, 1753−1757.

(90) Hortholary, C.; Minc, F.; Coudret, C.; Bonvoisin, J.; Launay, J. P. *Chem. Commun.* **2002**, 1932−1933.

(91) Weber, K.; Hockett, L.; Creager, S. *J. Phys. Chem.* **1997**, *101*, 8286−8291.

(92) Sumner, J. J.; Weber, K. S.; Hockett, L. A.; Creager, S. E. *J. Phys. Chem. B* **2000**, *104*, 7449−7454.

(93) Richardson, J. N.; Rowe, G. K.; Carter, M. T.; Tender, L. M.; Curtin, L. S.; Peck, S. R.; Murray, R. W. *Electrochim. Acta* **1995**, *40*, 1331−1338.

(94) Richardson, J. N.; Peck, S. R.; Curtin, L. S.; Tender, L. M.; Terrill, R. H.; Carter, M. T.; Murray, R. W.; Rowe, G. K.; Creager, S. E. *J. Phys. Chem.* **1995**, *99*, 766−772.